Research Article Vol. 40, No. 4 / April 2023 / Journal of the Optical Society of America B C1

Journal of the Optical Society of America B

OPTICAL PHYSICS

τ-algorithm for gathering spectroscopic information by modeling emission line shapes: application to laser-induced plasmas

D. M. Díaz Pace[1,*] and J. Molina M.[1,2]

[1]Centro de Investigaciones en Física e Ingeniería del Centro de la Provincia de Buenos Aires (CIFICEN), CONICET, CICPBA, Fac. Cs. Exactas, UNCPBA, Campus Universitario, (B7000GHG) Tandil, Buenos Aires, Argentina

[2]Mass Spectrometry & Optical Spectroscopy Group, Dpto. de Física, Escuela Politécnica Nacional (EPN), Ladrón de Guevara E11–253, Ed. #6, Piso 1, (170525) Quito, Ecuador

*Corresponding author: ddiaz@ifas.exa.unicen.edu.ar

Received 27 October 2022; revised 27 December 2022; accepted 3 January 2023; posted 5 January 2023; published 31 January 2023

In this work, a fitting algorithm was implemented and applied to analyze emission line shapes in laser-induced breakdown spectroscopy. By modeling emission spectral lines, the optical thickness was calculated for each line of interest and the intensity line profiles were computed and matched to measured spectra. The algorithm was applied to analyze the experimental profiles of a hydrogen H_α line at 6562.8 Å, and the resonant lines of Mg II at 2795.5 Å and at 2802.7 Å. Spectroscopic information was obtained about the physical processes occurring in the plasma, such as self-absorption and Stark broadening. The results demonstrated the potential of the developed method to provide valuable information in plasma spectroscopy for both fundamental and applied research.

https://doi.org/10.1364/JOSAB.479557

1. INTRODUCTION

The spectra from both astrophysical and laboratory plasmas contain a rich abundance of information about their physical characteristics [1]. This rewarding information can be recovered from the experimental data through a detailed analysis of the shape of the spectral lines measured from the source; i.e., a star or laboratory plasma. In this scenario, the feedback between fundamental and applied investigations results are of paramount importance to gather a deep understanding of the complex physicochemical processes involved in the plasma behavior. This feedback is crucial to optimize the measurement conditions to correctly interpret the results. Conversely, specifically designed experiments provide valuable input to refine the models of plasma radiation, which are substantially based in plasma physics [2].

Laser-induced breakdown spectroscopy (LIBS) is a well-suited technique for the spectroscopic study of laser-induced plasmas (LIP) in the laboratory. The LIBS method relies on the spectral analysis of the radiation emitted by a LIP, generated by ablation of the target material (gas, liquid, or solid), for the qualitative and quantitative determination of its chemical composition [3–5]. During the last decades, the outstanding technology development, mainly in lasers, detectors, and computers, made LIBS as a useful method to address rapid (<1 s), simultaneous, multi-elemental analysis with no need for a sample treatment. Moreover, the LIBS approach has several attractive advantages, in terms of simplicity and versatility, over conventional analytical techniques, which often require tedious and time-consuming sample preparation procedures. Consequently, LIBS spectroscopy is now a very active field of research with a wealth of appealing applications in a wide range of areas that include geology, cultural heritage, archaeology, environment, agriculture, industry, and spatial exploration [6].

For the study of LIPs generated in air at atmospheric pressure, the main issues that should be addressed are time evolution, spatial inhomogeneity, self-absorption, and matrix effects [7]. Self-absorption is always expected to be present at some degree in spectral radiation emerging from an extended source, such as a LIP. However, in general, spectral lines with a low to moderate degree of self-absorption can be hardly distinguished through only visual observation, even though they were measured with a high-resolution spectrometer; therefore, a more laborious analysis is required. Hence, a self-absorption assessment relies on two well-known effects on the line profile: (i) a reduction of its peak intensity; and (ii) an extra broadening of its observed FWHM. The recent review by Aberkane *et al*. [8] summarized the current state of the art on the main models of plasma radiation designed to determine fundamental spectral line parameters and coefficients in LIBS. In this review, several methods were discussed in which self-absorption of the spectral lines was checked and/or minimized to avoid systematic errors in the calculus. On the other hand, in another review by Rezaei *et al*. [9], the feasibility

of exploiting the self-absorption, instead of its reduction or prevention, was highlighted.

To the best of our knowledge, the so-called columnar density and C-sigma methods, developed by Cristoforetti and Tognoni [10] and Aragón and Aguilera [11], respectively, are the most relevant investigations reported in the pertinent literature regarding the exploitation of self-absorption of the lines to calculate the plasma/atomic parameters of spectroscopic interest using LIBS. Based on these steps, within a research project designed to contribute to the study of the shapes of emission spectral lines from LIBS, we adopted a different, but complementary, approach to the studies discussed above. In our approach, the self-absorption of the spectral lines is intrinsically considered. In previous works, we settled the basis of the method for modeling emission spectral lines to reproduce the spectra measured from laser-induced plasmas [12,13]. The optical thicknesses govern self-absorption, and they also could bring additional physical information that could be very useful for plasma characterization and for a more accurate calculation of the spectral parameters that cannot be easily determined in conventional LIBS analysis. In this work, the algorithm was revised and some bugs were amended, which resulted in a significantly improved and updated version. The capabilities of the model were assessed by applying it to experimental lines measured from LIBS experiments.

2. THEORETICAL

The basic equations that describe a radiating plasma, which is assumed to be homogenous, in local thermodynamic equilibrium (LTE), and cylinder-symmetrical, are remembered. The wavelength-dependent spectral intensity I_λ ($\mathrm{Wm^{-2}\,sr^{-1}\,nm^{-1}}$) along the line of sight is given by the solution to the equation of radiation transfer [14]:

$$I_\lambda = C U_\lambda \left(1 - e^{-\tau_\lambda(T)}\right), \tag{1}$$

where C (a.u.) is a factor that unifies units and depends on the instrumental setup, U_λ ($\mathrm{Wm^{-2}\,sr^{-1}\,nm^{-1}}$) is the Planck's distribution for blackbody radiation, T (K) is the plasma temperature, and τ_λ (dimensionless) is the optical thickness. The optical thickness can be separated into different factors [15], as

$$\tau_\lambda(T) = \kappa(\lambda) l = \kappa_e(T) N l\, P(\lambda), \tag{2}$$

where $\kappa_e(T)$ ($\mathrm{m^3}$) is a coefficient that depends on the atomic parameters of the transition. The coefficient $\kappa_e(T)$ can be calculated if the plasma temperature is known; namely,

$$\kappa_e(T) = \frac{\lambda_0^4}{8\pi c\, Q(T)} A_{ji} g_j e^{-E_i/kT} \left(1 - e^{E_i - E_j/kT}\right), \tag{3}$$

where λ_0(m) is the wavelength of the line, c ($\mathrm{m\,s^{-1}}$) is the speed of light in vacuum, A_{ji} ($\mathrm{s^{-1}}$) is the transition probability, g_j (dimensionless) is the degeneracy of the upper energy level, E_i, E_j (eV) are the energies of the levels, N ($\mathrm{m^{-3}}$) is the density of the emitting element in the plasma, l (m) is the length of the plasma along the line of sight, $P(\lambda)$ ($\mathrm{m^{-1}}$) is the normalized line shape, and $Q(T)$ (dimensionless) is the atomic partition function. The optical thickness governs the self-absorption of radiation within the plasma. It reaches a maximum τ_0 at the line center λ_0, and decreases toward the line wings. If the self-absorption is negligible, $\tau_0 \ll 1$, and the plasma is said to be optically thin. On the other hand, for more intense lines at higher concentrations, when the radiation emitted has a large probability of being absorbed, then, $\tau_0 \gg 1$, and the plasma is said to be optically thick. If τ_λ is known, the self-absorption correction factor R_λ (dimensionless) defined as in [16] can be obtained:

$$R_\lambda = \frac{I_\lambda^{\mathrm{thin}}}{I_\lambda} = \frac{\tau_\lambda}{1 - e^{-\tau_\lambda}}. \tag{4}$$

The correction factor R_λ can be applied to the measured lines to retrieve the optically thin line profiles for the same number density of emitters:

$$I_\lambda^{\mathrm{thin}} = R_\lambda I_\lambda. \tag{5}$$

To quantify the effect of self-absorption on the emission line intensity, a *SA* coefficient can be defined by calculating the ratio of the measured peak intensity over its value in the absence of self-absorption; namely,

$$SA \equiv 1 - \frac{I(\lambda_0)}{I^{\mathrm{thin}}(\lambda_0)} = 1 - \frac{1}{R_0}, \tag{6}$$

where R_0 is the value of R_λ at the line peak (λ_0). The *SA* coefficient can be expressed as a percentage by multiplying Eq. (6) by 100, in such a way that $SA = 0$ (or 0% absorbed) if the line is optically thin and it increases up to 1 (or 100%) as the line becomes self-absorbed. A more meaningful expression for *SA* can be derived by integrating the line intensities over the line shape,

$$SA_I \equiv 1 - \frac{\int_{\mathrm{line}} I_\lambda \mathrm{d}\lambda}{\int_{\mathrm{line}} I_\lambda^{\mathrm{thin}} \mathrm{d}\lambda} = 1 - \frac{I^{\mathrm{exp}}}{I^{\mathrm{thin}}}, \tag{7}$$

which accounts for the overall self-absorption of the line. In the equation above, I_{exp} is the measured net intensity, and I_{thin} is the net intensity in optically thin conditions.

3. EXPERIMENTAL

Two different setups, referred to as setup A and setup B, were employed for LIBS measurements. These setups have been previously used in [12,13,17], so only a brief description is given here. In both setups, a Nd:YAG laser (wavelength = 1064 nm, pulse width 4.5–7 ns, and pulse energy 60 mJ) was used to generate the plasmas in air at atmospheric pressure. The laser beam was focused with a quartz lens at right angles onto the sample surface. The plasma was imaged onto the entrance of a Czerny–Turner spectrometer. In setup A, the spectrometer (focal length 1.5 m, grating of 2400 lines $\mathrm{mm^{-1}}$, slit width 50 μm, and spectral resolution of 0.01 Å at 3000 Å) was equipped with a photomultiplier detector (Hamamatsu 1P28, spectral response range 2000–6000 Å) for time-resolved analysis and averaging of the signal. In setup B, the spectrometer (focal length 0.75 m, grating of 3600 lines $\mathrm{mm^{-1}}$, slit width 20 μm, and spectral resolution of 0.15 Å at 3000 Å) used a CCD detector (1200 × 256 effective pixels) to record the spectra. Both spectrometers

provided high spectral resolutions, providing instrumental broadening comparable to or less than the experimental line widths, which allowed the detailed measurement of the true line profiles.

Two experiments were devised in which the profiles of the H_α (at 6562.8 Å) and Mg II (at 2795.5 Å and 2802.7 Å) spectral lines were measured under appropriate experimental conditions for the purpose of this research. These lines were selected because they are isolated and free from interference from other elements. The spectroscopic data were taken from the National Institute of Standards and Technology (NIST) database [18]. Mg II lines were measured with setup A using samples prepared in the form of pellets of CaO with Mg concentrations in the range 62–625 ppm at a delay time of 7 μs from the laser pulse and with a fixed gate time of 1 μs. Due to the poor sensitivity of the photomultiplier detector in the visible region, the H_α line was measured with setup B from a fused glass disc with different time delays with respect to the laser pulse (ranging from 0.57 to 3.1 μs) and time widths (ranging from 0.06 to 0.6 μs). In both cases, the samples were rotated during the measurements and the emission from several laser shots was averaged to improve the SNR. To reduce the statistical error, each measurement was repeated at different sample locations and the resulting signal values were averaged. As described in Section 4, the experimental profiles of the measured lines were analyzed using a self-designed computational algorithm.

4. RESULTS AND DISCUSSION

A. Algorithm for Line Profile Analysis

The spectral line profile of a given transition along the line of sight is given by Eq. (1), which accounts for the processes of emission and absorption taking place inside the plasma plume. Therefore, the different broadening mechanisms existing in the LIP must be evaluated to calculate the intrinsic line profile $P(\lambda)$, as shown in Eq. (2); i.e., the Doppler effect and Stark effect. Moreover, self-absorption distorts the true shape; thus, $P(\lambda)$ is not described by a Lorentzian or a Voigt profile anymore. After that, the true shape should be convolved with the instrument profile. Finally, the C factor of Eq. (1) should be estimated to match the simulated to experimental profiles. At this point, it should be stressed that performing a direct calculus of the line intensity I_λ with Eqs. (1) and (2) is an unfeasible task. To do this requires an estimation of all the physical parameters, which depend on both the experimental conditions and plasma time evolution. In addition, computing a multiparametric fitting routine is clearly inefficient, highly time-consuming, and the different variables involved may compensate each other. Last, but not least, even if a tight fit of the data is obtained, it is not by itself a proof that the model is physically consistent.

To tackle the problem, an algorithm (termed τ-algorithm) was developed in the MATLAB environment to compute the emission spectra and match the spectra to the experimental profiles through a least-squares iterative fitting procedure. In a more feasible approach, it was based on the calculus of the optical thickness τ_λ of the lines of interest through the determination of two adjustable parameters; i.e., the maximum optical thickness (τ_0) and the Stark broadening (w_{Stark}). For a given line, the inputs are the experimental profile and its spectroscopic data. The fitting routine is run until the deviation of the synthetic from the experimental spectrum is minimized. The calculation time was less than 30 s. Hence, a profile that reproduces the measurements is obtained along with its wavelength-dependent optical thickness τ_λ. Finally, the self-absorption coefficient (SA_l) is evaluated and the experimental profile can be corrected for self-absorption, retrieving the optically thin line intensity. The errors in the least-squares fitting were the standard deviations of the fitted parameters calculated by using the bootstrap method [19]. To evaluate the performance of the algorithm, it was applied to cases that determined the electron density of the plasma, the study of self-absorption by means of the analysis of the curves of growth (CoG), as well as for the calculus of the Stark widths.

B. Electron Density

In the characterization of LIPs, the most widely used method to determine the electron density is based on the measurement of the Stark-broadened profiles of the reference lines with known values of their Stark widths. In most cases, the hydrogen emission line H_α is the line of choice [20]. Because the H_α line originates, in general, from the very low content of H in the humid air atmosphere in front of the target, it is assumed to be free of self-absorption. However, a possible self-absorption of the H_α line should be checked mainly during the last instants of plasma evolution. In fact, in the later stages of plasma evolution, a rapid drop in the plasma temperature brings a decrease of the electron density; consequently, the self-absorption may be stronger [12]. If self-absorption occurs, even at a low degree, it will cause a broadening of the line. which will originate an apparently larger Stark width and, thus, an overestimation of the electron density value. Therefore, the algorithm was applied to study the time evolution of the electron density of the plasma. The profile of the H_α line was analyzed in each case where the possible self-absorption of the line was evaluated, an accurate determination of its Stark width was performed, and a reliable value for the electron density was achieved. The electron density values of the plasma were calculated via the Stark widths of the H_α lines measured at different times of the plasma lifetime [7].

Due to the large Stark broadening of the H_α line, the spectral resolution of the spectrometer (setup B) allowed a detailed

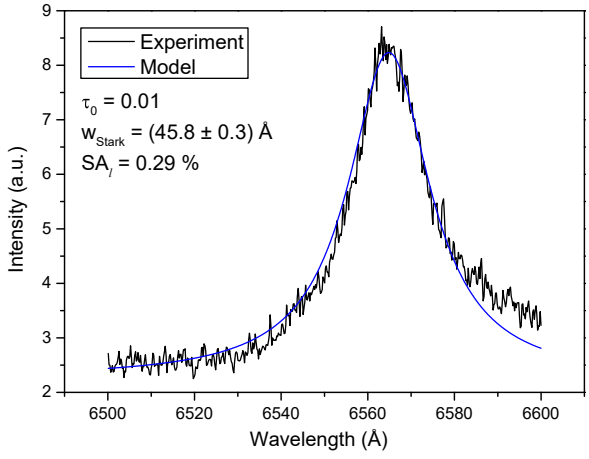

Fig. 1. Spectrum of the H_α line measured at a time of 1 μs and fitting model. The calculated parameters also are shown.

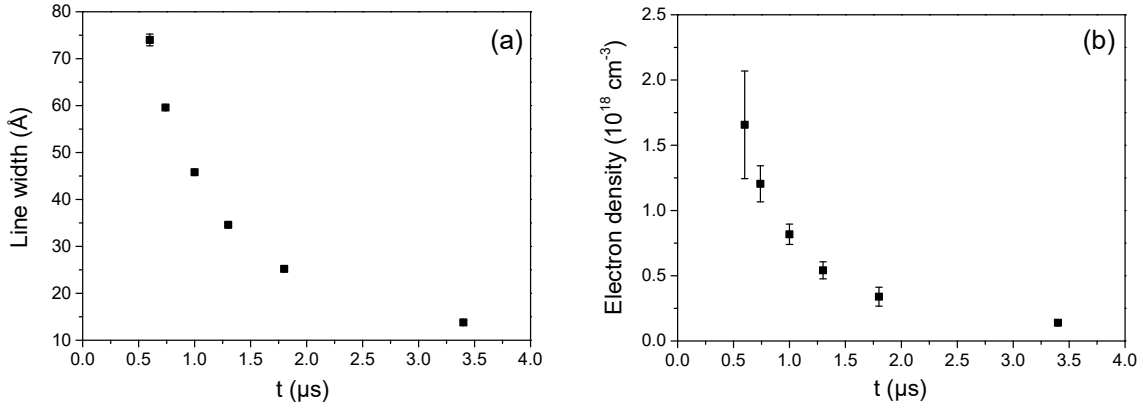

Fig. 2. (a) Stark width (w_{Stark}) of the H_α line and (b) electron density of the laser induced plasma measured at different instants of the plasma lifetime in the fused glass sample.

measurement of its line profile. For example, in Fig. 1 the H_α line measured at a delay time of 1 μs is shown, together with the fitting model and the obtained values for τ_0 and the SA_l coefficient. The self-absorption was less than 1% in all the measured times; thus, the line was emitted in optically thin conditions. The observed mean FWHM of the H_α lines was in the range $w_{\text{FWHM}} = (15-60 \pm 1)$ Å. The Doppler widths, estimated for a typical range of plasma temperatures (i.e., $kT \sim 1$ eV) were lower than $w_D \approx 0.50$ Å, while the instrument profile was represented by a Gaussian function with a fixed width $w_{\text{Instr}} \approx 1.40$ Å; therefore, w_D and w_{Instr} were neglected. Thus, in the algorithm, each experimental H_α line was fitted with an intrinsic shape given by a normalized Lorentzian profile related to the Stark broadening. The Stark widths, w_{Stark} (Å), of the H_α lines measured at the different times after the laser pulse were obtained [Fig. 2(a)], and the corresponding electron density values $N_e = (1.65-0.14) \times 10^{18}$ cm^{-3} were calculated, showing an exponential decay with time [Fig. 2(b)].

C. CoG

The CoG of a given emission line is defined as a graph of its intensity versus the different concentrations of the emitting element in the samples [11]. The algorithm was applied to the analysis of the experimental profiles of the Mg II resonant lines measured from samples with different Mg content at a fixed instant of plasma evolution. Here, the optical depth of the line varied due to the change in the corresponding number density of the species in the plasma. An example is shown in Fig. 3. The observed mean FWHM of the Mg II lines was in the range $w_{\text{FWHM}} = (0.10-0.19 \pm 0.02)$ Å. The Doppler width, estimated for a plasma temperature of 1 eV was $w_D = 0.044$ Å, while the instrument width was $w_{\text{Instr}} = 0.065$ Å; thus, w_D and w_{Instr} were neglected and the intrinsic shapes were given by normalized Lorentzian profiles related to the Stark broadening w_{Stark}. The measured extra broadening of the lines, given by w_{FWHM} with respect to w_{Stark}, was due to self-absorption.

The optical thicknesses were calculated, and the self-absorption was evaluated and compensated. The CoG curves obtained with the wavelength-integrated emission intensities are shown in Fig. 4 (solid circles). A linear dependence of the intensities was observed at low concentrations where the plasma

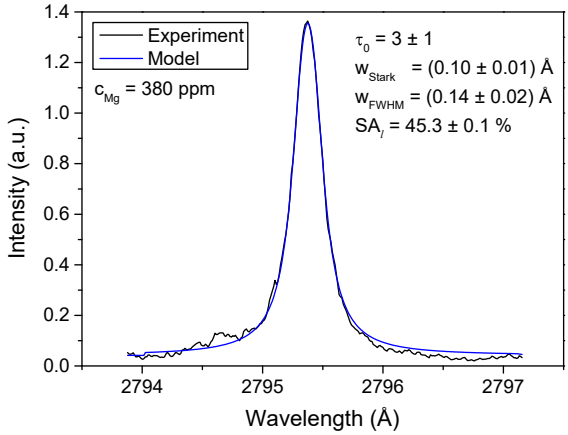

Fig. 3. Spectrum of the 2795.5 Mg II line measured at a time of 7 μs and fitting model for the sample with 380 ppm of Mg. The calculated physical parameters are shown.

is optically thin, while saturation was progressively reached at increasing concentrations, as the plasma becomes optically thick, and a strong self-absorption occurs at higher concentrations. The experimental intensity data were fitted with the nonlinear function proposed in [21]:

$$y = a + bc(1 - e^{-x/c}), \tag{8}$$

where x represents the elemental concentration and y is the line intensity. Physically, the parameter c refers to the critical concentration at which self-absorption of the line becomes noticeable. For concentrations lower than c ($x < c$), Eq. (8) reduces to

$$y = a + bx, \tag{9}$$

which gives the linear trend observed for the optically thin regime. Self-absorption correction was carried out to retrieve the optically thin line intensities, which are also included in Fig. 4 (open squares). The negative value at x axis (i.e., $x_0 = -a/b$) indicated a preexisting Mg concentration of $c_0^{\text{Mg}} = (85 \pm 11)$ ppm in the samples. Figure 4 shows that the line intensities corrected for self-absorption fit well with the predictions of Eq. (9), within the experimental error.

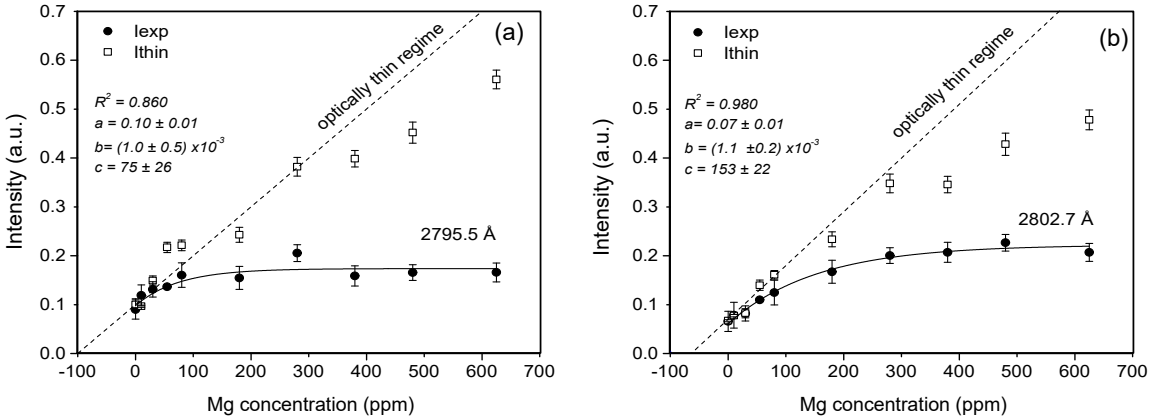

Fig. 4. Experimental CoG curves of Mg II resonant lines: (a) 2795.5 Å and (b) 2802.7 Å, and fitting curve.

At higher concentrations (≥400 ppm) of Mg, however, the line intensities were lower than the values predicted by the model. This observation can be explained by the fact that the adopted model of a homogeneous plasma was not able to account satisfactorily for the high concentration region of CoG curves constructed with the most intense lines, as described by Aragón and Aguilera in [11]. A more realistic model could be used; nevertheless, the models of inhomogeneous plasmas are complex and time consuming, which may reduce their practical applicability [21]. The temperature of the plasma was measured using the Boltzmann plot method applied to four Mg II lines (i.e., 2790.8 Å, 2795.5 Å, 2798.0 Å, and 2802.7 Å). The use of Mg II lines, for which precise data of the transition probabilities are available, allowed accurate temperature values to be obtained. The electron density was obtained from the Stark broadening of the resonant Mg II lines. The values of the temperature, $kT = (0.95 \pm 0.4)$ eV, and of the electron density, $N_e = (4.6 \pm 0.9) \times 10^{17}$ cm^{-3}, that were obtained for the samples with the different Mg concentrations in the $Ca(OH)_2$ matrices were the same within the experimental errors. This is evidence that chemical matrix effect was negligible in our experiment.

D. Stark Widths

In Fig. 5(a), the obtained maximum values τ_0 for the Mg II lines are plotted as a function of the Mg concentration, considering its initial content. Linear trends with a zero intercept were observed, which corresponded to the expected growth of the optical thicknesses of the lines, being proportional to the increment of the Mg content in the samples [see Eq. (2)]. In addition, the optical thickness of the line 2795.5 Å was larger than that of the line 2802.7 Å, which agrees with the observance in Fig. 4 that the change from an optically thin to an optically thick regime, given by the c parameter of Eq. (8), is more abrupt for the first line (75 ppm) than for the second line (153 ppm). This implies that the former is more sensitive to self-absorption.

A well-known procedure to evaluate self-absorption is checking the intensity ratio of a pair of spectral lines belonging to the same multiplet. For these lines, the Stark widths of spectral lines belonging to the same multiplet are usually the same within a few percentage points [22]. Thus, the lines of the Mg II doublet have approximately the same line profiles in Eq. (2). In this work, since self-absorption is governed by the optical thickness, we employed the calculated maximum values of the optical thicknesses of the Mg II doublet to evaluate the relative self-absorption. The relative self-absorption is determined only by their κ_e coefficients, which depend on their spectroscopic features and the plasma temperature. In our case, $\kappa_e^{2795.5}/\kappa_e^{2802.7} = \tau_0^{2795.5}/\tau_0^{2802.7} \approx 2$, independent of the temperature, and it is mainly given by the degeneracy of the excited states of the transitions (i.e., $g_j = 4$ and 2, respectively). Therefore, it is deduced that line 2795.5 Å is approximately two times more sensitive to self-absorption than line 2802.7 Å. This conclusion agreed with the mean ratio of 1.8 ± 0.6 obtained in our experiment.

To check the validity of the algorithm to accurately calculate the Stark widths, the Lorentzian widths of the intrinsic shapes of the Mg II lines were plotted as a function of the Mg concentration. The results are shown in Fig. 5(b) for line 2802.7 Å, where the FWHM of the lines are also included for comparison. It was observed that the FWHM increased with concentration due to a corresponding increment in the self-absorption of the lines, while the Lorentzian widths, related to Stark broadening, remained constant, except for the highest concentration where the homogeneous plasma model failed. The final value for the Stark width $w_{\text{Stark}} = (0.12 \pm 0.01)$ Å was obtained as the average, discarding the last value when the homogeneous plasma model failed. Since self-absorption causes an additional broadening of the line profiles with respect to the optically thin case, it is observed that line 279.55 nm will experience a faster broadening than line 280.27 nm as the Mg density grows.

It should be stressed that the results presented here, as well as in the previous sections, have been derived from the spectra obtained by integration of the measured emission intensity along the line of sight from a "near homogeneous" plasma, where the gradient effects of temperature and species densities on the line profiles were neglected. Therefore, the optical thicknesses as well as the plasma parameters calculated are, in fact, apparent values corresponding to population-averaged local values.

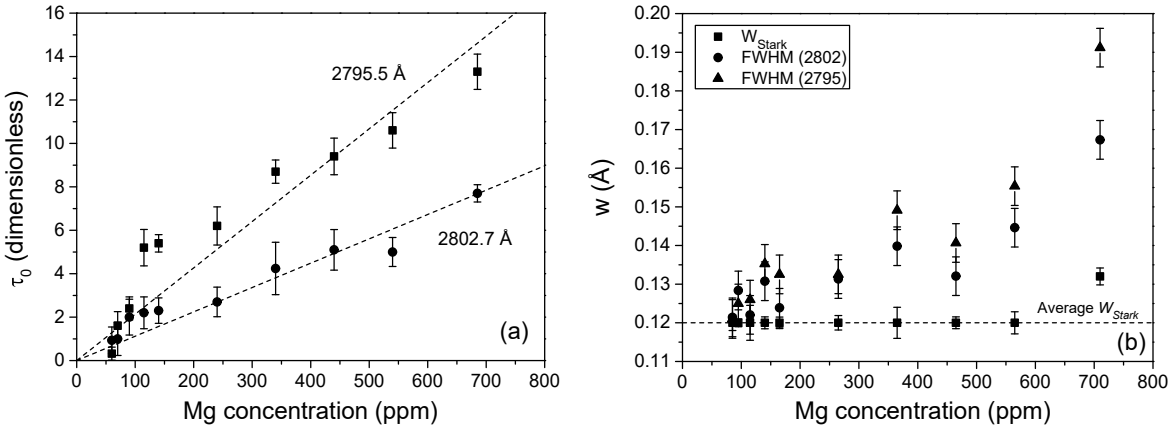

Fig. 5. (a) Maximum optical thicknesses of 2795.5 Å and 2802.7 Å Mg II lines and fitting curve, and (b) line widths measured as a function of the Mg concentration.

5. CONCLUSION

In this paper, the shapes of suitable spectral lines were analyzed using what we believe, to the best of our knowledge, is a new and improved fitting algorithm to model emission line shapes. The performance of the algorithm was evaluated by applying it to the emission intensity profiles of a H_α line and resonant Mg II lines measured with good resolution and spatially integrated along the line of observation. From the individual analysis of these lines, useful insights for plasma characterization were extracted, including the optical thickness, self-absorption evaluation and compensation, electron density calculation, CoG features, and accurate determination of Stark broadenings. The values obtained for the plasma parameters and the optical thicknesses were apparent values corresponding to population-averaged local values. The obtained results demonstrated the high potential of the developed method to recover the information saved in the optical thicknesses of the spectral lines and that it can be effectively used in the study of the plasmas generated in LIBS experiments. Compared to other reported models, it allows the calculation of the wavelength-dependent optical thicknesses without requiring CoG construction since one sample is sufficient to achieve a reliable plasma characterization. In addition, the spectral lines without known Stark coefficients also can be analyzed. This model is practical and fast, with a calculation time of less than 30 s for each line. It also is comprehensive, which means that it can properly address the observed spectral features. Finally, the general methodology can be further extended to other atomic/ionic elements as well as to astronomical spectra, suggesting a great potential in spectroscopic applications.

Funding. Consejo Nacional de Investigaciones Científicas y Técnicas (CONICET) of Argentina.

Acknowledgment. J. A. Aguilera and C. Aragón from the Department of Sciences at UPNA University are greatly acknowledged.

Disclosures. The authors declare no conflict of interest.

Data availability. Data underlying the results presented in this paper are not publicly available at this time but may be obtained from the authors upon reasonable request.

REFERENCES

1. A. Thorne, U. Litzén, and S. Johansson, "The width and shape of spectral lines," in *Spectrophysics: Principles and Applications* (Springer, 1999), pp. 187–208.
2. H. R. Griem, *Plasma Spectroscopy* (McGraw-Hill, 1964).
3. A. W. Miziolek, V. Palleschi, and I. Schechter, *Laser Induced Breakdown Spectroscopy* (Cambridge University, 2006).
4. D. A. Cremers and L. J. Radziemski, *Handbook of Laser-Induced Breakdown Spectroscopy* (Wiley, 2006).
5. J. P. Singh and S. N. Thakur, *Laser-Induced Breakdown Spectroscopy* (Elsevier, 2007).
6. D. W. Hahn and N. Omenetto, "Laser-induced breakdown spectroscopy (LIBS), Part II: review of instrumental and methodological approaches to material analysis and applications to different fields," Appl. Spectrosc. **66**, 347–419 (2012).
7. C. Aragón and J. A. Aguilera, "Characterization of laser induced plasmas by optical emission spectroscopy: A review of experiments and methods," Spectrochim. Acta B **63**, 893–916 (2008).
8. S. Messaoud Aberkane, A. Safi, A. Botto, B. Campanella, S. Legnaioli, F. Poggialini, S. Raneri, F. Rezaei, and V. Palleschi, "Laser-induced breakdown spectroscopy for determination of spectral fundamental parameters," Appl. Sci. **10**, 4973 (2020).
9. F. Rezaei, G. Cristoforetti, E. Tognoni, S. Legnaioli, V. Palleschi, and A. Safi, "A review of the current analytical approaches for evaluating, compensating and exploiting self-absorption in Laser Induced Breakdown Spectroscopy," Spectrochim. Acta B **169**, 105878 (2020).
10. G. Cristoforetti and E. Tognoni, "Calculation of elemental columnar density from self-absorbed lines in laser-induced breakdown spectroscopy: a resource for quantitative analysis," Spectrochim. Acta B **79–80**, 63–71 (2013).
11. C. Aragón and J. A. Aguilera, "CSigma graphs: A new approach for plasma characterization in laser-induced breakdown spectroscopy," J. Quant. Spectrosc. Radiat. Transf. **149**, 90–102 (2014).
12. D. M. Díaz Pace, C. A. D'Angelo, and G. Bertuccelli, "Study of self-absorption of emission magnesium lines in laser-induced plasmas on calcium hydroxide matrix," IEEE Trans. Plasma Sci. **40**, 898–908 (2012).
13. D. M. Díaz Pace, C. A. D'Angelo, and G. Bertuccelli, "Calculation of optical thicknesses of magnesium emission spectral lines for diagnostics of laser-induced plasmas," Appl. Spectrosc. **65**, 1202–1212 (2011).
14. H. Zwicker, "Evaluation of plasma parameters in optically thick plasmas," in *Plasma Diagnostics*, W. Lochte-Holtgreven, ed. (North-Holland Publishing, 1968), pp. 214–248.
15. C. Aragón, J. Bengoechea, and J. A. Aguilera, "Influence of the optical depth on spectral line emission from laser-induced plasmas," Spectrochim. Acta B **56**, 619–628 (2001).

16. H. Y. Moon, K. K. Herrera, N. Omenetto, B. W. Smith, and J. D. Winefordner, "On the usefulness of a duplicating mirror to evaluate self-absorption effects in laser induced breakdown spectroscopy," Spectrochim. Acta B **64**, 702–713 (2009).
17. J. Manrique, D. M. Díaz Pace, C. Aragón, and J. A. Aguilera, "Experimental stark widths and shifts of V II spectral lines," Mon. Not. R. Astron. Soc. **498**, 2068–2074 (2020).
18. NIST Physical Measurement Laboratory, "Atomic spectra database," (version 5.10), https://www.nist.gov/pml/atomic-spectra-database.
19. T. C. O'Haver, "A pragmatic introduction to signal processing," University of Maryland (updated January 2023), https://terpconnect.umd.edu/~toh/spectrum/.
20. C. Aragón and J. A. Aguilera, "Determination of the local electron number density in laser-induced plasmas by Stark-broadened profiles of spectral lines comparative results from Hα, Fe I and Si II lines," Spectrochim. Acta B **65**, 395–400 (2010).
21. D. M. Díaz Pace, C. A. D'Angelo, and G. Bertuccelli, "Semiempirical model for analysis of inhomogeneous optically thick laser-induced plasmas," Spectrochim. Acta B **64**, 999–1008 (2009).
22. N. Konjevic, M. Ivkovic, and S. Jovicevic, "Spectroscopic diagnostics of laser-induced plasmas," Spectrochim. Acta B **65**, 593–602 (2010).